

Surface Inactivation of Highly Mutated SARS-CoV-2 Variants of Concern: Alpha, Delta, and Omicron

Valentin A. Bobrin,[§] Sung-Po R. Chen,[§] Carlos Fitzgerald Grandes Reyes, Tim Smith, Damian F. J. Purcell, Jason Armstrong, Julie L. McAuley, and Michael J. Monteiro*



Cite This: *Biomacromolecules* 2022, 23, 3960–3967



Read Online

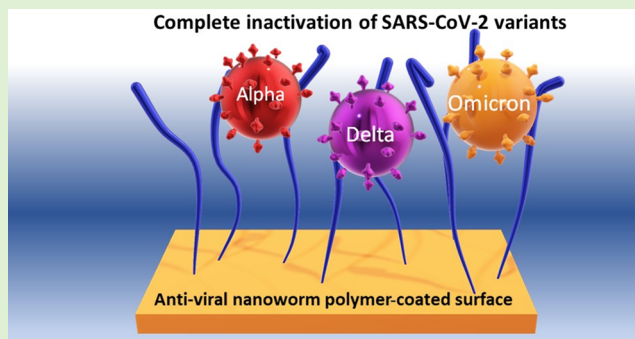
ACCESS |

 Metrics & More

 Article Recommendations

 Supporting Information

ABSTRACT: Continued SARS-CoV-2 transmission among the human population has meant the evolution of the virus to produce variants of increased infectiousness and virulence, coined variants of concern (VOCs). The last wave of pandemic infections was driven predominantly by the delta VOC, but because of continued transmission and adaptive mutations, the more highly transmissible omicron variant emerged and is now dominant. However, due to waning immunity and emergence of new variants, vaccines alone cannot control the pandemic. The application of an antiviral coating to high-touch surfaces and physical barriers such as masks are an effective means to inactivate the virus and their spread. Here, we demonstrate an environmentally friendly water-borne polymer coating that can completely inactivate SARS-CoV-2 independent of the infectious variant. The polymer was designed to target the highly glycosylated spike protein on the virion surface and inactivate the virion by disruption of the viral membrane through a nano-mechanical process. Our findings show that, even with low amounts of coating on the surface (1 g/m²), inactivation of alpha, delta, and omicron VOCs and degradation of their viral genome were complete. Furthermore, our data shows that the polymer induces little to no skin sensitization in mice and is non-toxic upon oral ingestion in rats. We anticipate that our transparent polymer coating can be applied to face masks and many other surfaces to capture and inactivate the virus, aiding in the reduction of SARS-CoV-2 transmission and evolution of new variants of concern.



INTRODUCTION

Vaccination against severe acute respiratory syndrome coronavirus 2 (SARS-CoV-2) has significantly reduced the severity of the coronavirus infectious disease (COVID-19). Yet, the virus is still transmitting rampantly around the globe. The resurgence of COVID-19 across many vaccinated countries with high levels of vaccination in their population may be due to the decrease in protective antibody titers after 5–7 months post second dose^{1–3} and the evolution of new variants. The fourth wave was originally dominated by the delta (B.1.617.2) variant of concern (VOC); however, the more transmissible omicron (B.1.1.529) VOC has become the dominant SARS-CoV-2 isolate infecting people.^{1–3} Omicron is the fifth SARS-CoV-2 variant to be named by the World Health Organization, following the Alpha (B.1.1.7), Beta (B.1.351), Gamma (P.1), and Delta (B.1.617.2) variants. Clearly, vaccines alone are failing to control the spread of the virus. In addition to behavioral changes, such as isolating when infectious, more must be done to reduce the transmission rates. The challenge is to develop a protective system that can be rapidly implemented across the globe to stem the transmission of the virus and provide time for deployment and development of vaccines and antiviral drugs.

SARS-CoV-2 evolutionary mutations during adaptation to the human host have imparted a functional viral fitness advantage that has resulted in increased transmission potential,⁴ enhanced disease severity,^{5,6} aided immune evasion,⁷ and reduced sensitivity to neutralizing antibodies.⁸ These mutations, particularly in the spike protein at sites required for viral attachment to its host-receptor ACE2, provided the alpha (B.1.1.7) and the delta (B.1.617.2) VOCs with a replicative advantage⁹ over the ancestral isolates, including enhanced affinity for ACE2.^{10,11} This improved ACE2 affinity enables the virus to rapidly enter and egress viral progeny from cells and thus confer the advantage of the ability of the virus to spread more efficiently.^{4,6,12} Furthermore, once the alpha and delta VOCs bind to ACE2, the mutations located close to the spike S1/S2 region further enhance cleavage by the serine proteinase (TMPRSS2) on the cell

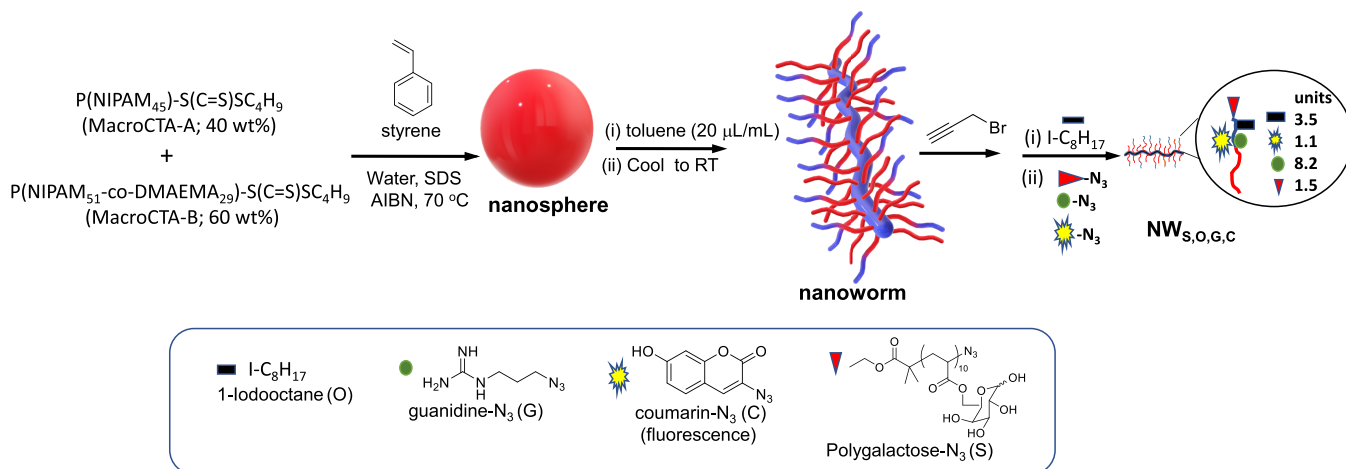
Received: June 27, 2022

Revised: August 4, 2022

Published: August 22, 2022



Scheme 1. Synthesis of the Functional Nanoworms through the Environmentally Friendly Emulsion Polymerization Method and Post-Modification with Chemically Functional Groups for Capturing (Polygalactose) and Rupturing (Octane Groups) of SARS-CoV-2, Degradation of its mRNA (Guanidine Groups), and Detection of Polymer Coating (Coumarin Groups)



surface, more rapidly exposing the hydrophobic region of the spike protein to fuse with the endosomal membrane and release of the viral RNA within the cell.^{13,14}

Regardless of their vaccination status, infected persons can release SARS-CoV-2 into the environment via sneezing, coughing, and skin contact, resulting in potential fomite contamination of surrounding surfaces.^{15–18} Infectious SARS-CoV-2 has been proven in laboratory-based studies to persist on many different surfaces.^{16,19,20} Personal protective equipment (e.g., face masks), treatment of high-touch surfaces with long-lasting antiviral coatings, and disinfection of contaminated surfaces are requirements to reduce the spread of SARS-CoV-2.²¹ We previously developed an environmentally friendly water-borne antiviral coating consisting of environmentally responsive polymer nanostructures and evaluated their effectiveness against respiratory viruses.²² For this study, we demonstrate the ability to synthesize functional polymer nanoworms (Scheme 1) amenable for industry manufacturing, prove maintenance of complete virucidal activity against further VOCs while limiting the amount of polymer on the surface, and provide evidence for the non-toxic nature of the polymer.

EXPERIMENTAL SECTION

Instrumentation. Nuclear Magnetic Resonance (NMR). All NMR spectra were recorded on either Bruker DRX 400 or 500 MHz spectrometers using an external lock (CDCl₃, DMSO-*d*₆, or D₂O).

Size Exclusion Chromatography (SEC) and Triple Detection-Size Exclusion Chromatography (TD-SEC). Analysis of the molecular weight distributions of the polymers was determined using a Polymer Laboratories GPC50 Plus equipped with a differential refractive index detector. Absolute molecular weights of polymers were determined using a Polymer Laboratories GPC50 Plus equipped with dual-angle laser light scattering detector, viscometer, and differential refractive index detector. HPLC grade *N,N*-dimethylacetamide (DMAc, containing 0.03 wt % LiCl) was used as the eluent at a flow rate of 1.0 mL/min. Separations were achieved using two PLGel Mixed B (7.8 × 300 mm) SEC columns connected in series and held at a constant temperature of 50 °C. InfinityLab EasiVial polystyrene standards were used for SEC column calibration. Samples of known concentration were freshly prepared in DMAc +0.03 wt % LiCl and passed through a 0.45 μm PTFE syringe filter prior to injection. The absolute molecular weights and dn/dc values were determined using

Polymer Laboratories Multi Cirrus software based on the quantitative mass recovery technique.

Dynamic Light Scattering (DLS). The size and zeta potential of particles were measured by DLS, which was performed using a Malvern Zetasizer Nano Series running DTS software and operating a 4 mW He-Ne laser at 633 nm. Analysis was performed at an angle of 173° and a constant temperature of 25 °C. The number-average hydrodynamic particle size and PDI_(DLS) were reported. The PDI_(DLS) was used to describe the width of the particle size distribution and calculated from a cumulant analysis of the DLS measured intensity autocorrelation function and is related to the standard deviation of the hypothetical Gaussian distribution (i.e., PDI_(DLS) = σ^2/Z_D^2 , where σ is the standard deviation and Z_D is the Z average mean size).

Transmission Electron Microscopy (TEM). The nanostructure appearance was determined using a HT-7700 transmission electron microscope utilizing an accelerating voltage of 80 kV with a spot size of 1 at ambient temperature. A typical TEM grid preparation was as follows: A sample was diluted with Milli-Q water to approximately 0.02–0.05 wt % at room temperature. A formvar precoated copper TEM grid was dipped into the solution, and the excess aliquot was blotted and then allowed to air dry prior to imaging on TEM.

Attenuated Total Reflectance-Fourier Transform Spectroscopy (ATR-FTIR). ATR-FTIR spectra were obtained using a horizontal, single bounce, diamond ATR accessory on a Nicolet Nexus 870 FT-IR. Spectra were recorded between 4000 and 500 cm⁻¹ for 32 scans at 4 cm⁻¹ resolution with an OPD velocity of 0.6289 cm s⁻¹. Solids were pressed directly onto the diamond internal reflection element of the ATR without further sample preparation.

Synthesis of Multifunctional Nanoworms (NWs). **Synthesis of Base Nanoworms (NW_{base}).** MacroCTA-A in EtOH (27.1028 g, 2.02 × 10⁻³ mol), MacroCTA-B in EtOH (30.1925 g, 1.58 × 10⁻³ mol), SDS (1.1229 g, 3.89 × 10⁻³ mol), and 460 mL of cold Milli-Q H₂O were added to a reactor under an argon blanket. The solution was stirred at 250 rpm in an ice bath until all components dissolved. The stirring rate was decreased to 50 rpm. AIBN (0.0887 g, 5.40 × 10⁻⁴ mol) was dissolved in STY (20.9936 g, 2.02 × 10⁻¹ mol), and the solution was added to the reaction under an argon blanket. The reaction solution was degassed by bubbling with argon for 120 min. The stirring rate was increased to 250 rpm, then the reactor was heated to 70 °C in a temperature-controlled oil bath, and the emulsion polymerization was allowed to proceed. After 4 h, ~0.1 mL of the polymer latex was taken and characterized by ¹H NMR (to determine the conversion of STY), and the reaction was quenched by exposing the reactor to air after 5 h. A sample was taken, freeze-dried, and later characterized by ¹H NMR and SEC (to determine the final conversion and M_n). The volatiles were removed by applying a gentle compressed air flow while stirring at 70 °C for 2 h. A sample was

taken and characterized by DLS (to determine the particle size). To transform the polymer latex to nanoworms, the stirring rate was decreased to 50 rpm and toluene (8.6750 g, 20 $\mu\text{L}/\text{mL}$) was added. The reactor was then removed from heating and allowed to cool to ambient temperature, taking ~ 24 h. Toluene was removed from the latex dispersion (500 mL) via rotary evaporation at 22 $^{\circ}\text{C}$ (25–50 mbar pressure) for ~ 3 h, in which the nanoworms kept their morphology (see Figure S13 in the Supporting Information).

Quaternization of NW_{base} with Iodoctane and Propargyl Bromide (QPO- NW_{base}). A small amount of NW_{base} in water (0.4 mL) was freeze-dried (three repeats) to determine the wt % of NW_{base} . It was found that the wt % of NW_{base} was 7.5 wt %. The required amounts of iodoctane, propargyl bromide, and DMSO were determined from this wt %. Accordingly, 36 mL of Milli-Q water was added to NW_{base} aqueous dispersion (34.23 g of NW_{base} in 420 mL of Milli-Q water). Iodoctane (1.0497 g) in 56.3 mL of DMSO was added to NW_{base} aqueous dispersion, and the reaction mixture was stirred in a 1 L glass Schott bottle for 15 h at 23 $^{\circ}\text{C}$. Then, 2.5 g of propargyl bromide (80 wt % in toluene) in 24.14 mL of DMSO was added to the NW_{base} reaction mixture and the reaction was carried out for an additional 12 h at 23 $^{\circ}\text{C}$. The reaction mixture was dialyzed (3500 MWCO) against Milli-Q water in a 5 L beaker for 24 h (changed Milli-Q water four times, approximately every 6 h) to remove unreacted iodoctane and propargyl bromide. After dialysis, the product QPO- NW_{base} was transferred to a 1 L Schott bottle. A small amount of QPO- NW_{base} was freeze-dried (three Eppendorf tubes with 0.4 mL each) to calculate the wt % of solid in the final dispersion.

Synthesis of $\text{NW}_{\text{S,O,G,C}}$. A small amount of QPO- NW_{base} in water (0.4 mL) was freeze-dried (three repeats) to determine the wt % of QPO- NW_{base} . It was found that the wt % of QPO- NW_{base} was 3.9 wt %. Based on this value, the amounts of guanidine azide, polygalactose azide, coumarin azide, copper sulfate, ascorbic acid, and DMSO to be added to the nanoworms were determined. Accordingly, 614 mL of 3.9 wt % QPO- NW_{base} dispersion (containing 25 g of QPO- NW_{base} solid) was placed in a 2 L two-neck round bottom flask. The following solutions were added to the flask: (i) guanidine azide (1.13 g) in 39.6 mL of DMSO, (ii) 3-azido-7-hydroxycoumarin (0.1796 g) in 39.6 mL of DMSO, and (iii) polygalactose azide (2.98 g) in 39.6 mL of DMSO. The resulting dispersion was purged with argon for 6 h. Ascorbic acid (10.89 g) in degassed Milli-Q water (35 mL, purged with argon for 2 h) was then injected into the reaction mixture in the flask via a degassed syringe followed by the injection of copper sulfate (4.23 g) in degassed Milli-Q water (25 mL, purged with argon for 2 h). The reaction was carried out for 19 h at 23 $^{\circ}\text{C}$ under an argon atmosphere in the dark. The reaction was stopped by exposure to the air and addition of 7 g of aluminum basic oxide (0.5 g) and stirred for 2 h. Aluminum oxide particles settled down to the bottom of the flask, and the nanoworm dispersion was decanted to a 1 L bottle. The nanoworm dispersion was dialyzed against Milli-Q water (3500 MWCO, water was changed every 3 h, and dialysis bags were changed to new ones after 8 h) in a 3 L beaker for 17 h. The resulting solution was freeze-dried to obtain $\text{NW}_{\text{S,O,G,C}}$ as a light yellowish powder. Zeta-potential (2 mg/mL, 25 $^{\circ}\text{C}$, Milli-Q water) = +26.5 mV.

Coating and Droplet Spreading of the Armrest Surface. A dispersion of $\text{NW}_{\text{S,O,G,C}}$ at 1.5 wt % in 70% autoclave water and 30% ethanol was prepared. An armrest (1 cm \times 1 cm) was cleaned by wiping with 100% ethanol followed by wiping with Milli-Q water and drying at ambient temperature. $\text{NW}_{\text{S,O,G,C}}$ dispersion was sprayed onto an armrest at a distance of approximately 7 cm from an armrest. The armrest was dried completely by gently blowing with an air dryer. The spraying-drying cycle was repeated four times. A 10 μL solution of either 0.2 M PBS solution at pH 6.5 or 7.4 and 23 $^{\circ}\text{C}$ was placed on an uncoated armrest (1 cm \times 1 cm) or on a $\text{NW}_{\text{S,O,G,C}}$ -coated armrest (1 cm \times 1 cm) at 23 $^{\circ}\text{C}$. Photographs of droplet spreading were taken at 5 and 30 min after the droplet addition.

Surface Testing for Virucidal Activity against SARS-CoV-2. All SARS-CoV-2 infection cultures were conducted within the high containment facilities in a PC3 laboratory at the Doherty Institute. Stocks of SARS-CoV-2 isolate hCoV-19/Australia/VIC17991/2020

(B.1.1.7 variant) and VIC18440 (Indian-2, delta variant) were produced from infected Vero cell supernatants. The genomic sequence of each stock of SARS-CoV-2 isolate was confirmed to match the publicly available data of the original virus isolate (www.gisaid.org, accession numbers: EPI_ISL_779606 and EPI_ISL_1913206, respectively).

Virus inoculum was created by adding an equal volume of virus stocks to filtered sterilized Sorensen's pH buffer at pH = 6.5. Then, 50 μL of inoculum was added dropwise to the surface of each material and allowed to incubate at room temperature for the duration specified. The surface of each material was then washed eight times by pipetting with 500 μL infection media, with care taken not to scratch the surface. The eluate was then collected, and the infectious virus titer was quantified via a 50% tissue culture infectious dose (TCID₅₀) assay using the appropriate cell line (Vero cells for SARS-CoV-2). Viral RNA was also extracted from the eluate using a QiaAmp Viral RNA extraction kit (Qiagen, Australia) as per the manufacturer's instructions and stored at -80°C . To evaluate the amount of virus genome present in each sample, we performed a quantitative reverse-transcription PCR (qRT-PCR) for detection of the SARS-CoV-2 envelope (E) gene and influenza nucleoprotein (NP) gene segment. Using the SuperScriptIII OneStep RT-PCR System with Platinum Taq DNA Polymerase (Invitrogen, Carlsband, CA, USA), the RT-qPCR assay composed of 5 μL of RNA, 12.5 μL of 2 \times Reaction Master Mix, 0.4 μL of 50 mM MgSO₄, 1 μL of Superscript III/Taq Enzyme Mix, 0.4 μM forward and reverse primers, 0.2 μM primer probe (using previously published primer-probe sequences²³), 1 μL of 1 mg/mL bovine serum albumin (BSA), and 2.6 μL of RNase free H₂O. The RT-qPCR assay was performed on a Bio-Rad CFX96 Touch real-time PCR detection system (Bio-Rad, Hercules, CA, USA) using the following conditions: a denaturation step at 55 $^{\circ}\text{C}$ for 10 min and 95 $^{\circ}\text{C}$ for 3 min followed by 45 cycles of amplification (94 $^{\circ}\text{C}$ for 15 s and 58 $^{\circ}\text{C}$ for 30 s). A known amount of influenza A virus and SARS-CoV-2 RNA (generated previously from virus stock cultures) diluted two-fold was used to generate a standard curve. The Ct values from the standard curve were used to interpolate the amount of SARS-CoV-2 RNA in each of the samples.

Surface Exposure Assay. SARS-CoV-2 inoculum was created by adding an equal volume of virus stocks to filter sterilized Sorensen's pH buffer at pH = 6.5. Inoculum (50 μL) was then added dropwise to the surface of each material and then allowed to incubate at room temperature for the duration specified. The surface of each material was then washed eight times by pipetting with 500 μL infection media, with care taken not to scratch the surface. The eluate was then collected, and the infectious virus titer was quantified via a 50% tissue culture infectious dose (TCID₅₀) assay. Viral RNA was also extracted from the eluate using the QiaAmp Viral RNA extraction kit (Qiagen, Australia) as per the manufacturer's instructions and stored at -80°C . To evaluate the amount of virus genome present in each sample, we performed a reverse-transcription quantitative PCR (RT-qPCR) for detection of the SARS-CoV-2 envelope (E) gene. Using the SuperScriptIII OneStep RT-PCR System with Platinum Taq DNA Polymerase (Invitrogen, Carlsband, CA, USA), the RT-qPCR assay composed of 5 μL of RNA, 12.5 μL of 2 \times Reaction Master Mix, 0.4 μL of 50 mM MgSO₄, 1 μL of Superscript III/Taq Enzyme Mix, 0.4 μM forward (5'-ACAGGTACGTTAATAGTTAATAGCGT-3') and 0.4 μM reverse (5'-ATATTGCAGCAGTACGCACACA-3') primers, 0.2 μM primer probe (5'-FAM-ACACTAGCCATCCT-TACTGCGCTTCG-BBQ-3'), 1 μL of 1 mg/mL bovine serum albumin (BSA), and 2.6 μL of RNase free H₂O. The RT-qPCR assay was performed on a Bio-Rad CFX96 Touch real-time PCR detection system (Bio-Rad, Hercules, CA, USA) using the following conditions: a denaturation step at 55 $^{\circ}\text{C}$ for 10 min and 95 $^{\circ}\text{C}$ for 3 min followed by 45 cycles of amplification (94 $^{\circ}\text{C}$ for 15 s and 58 $^{\circ}\text{C}$ for 30 s). A known amount of SARS-CoV-2 RNA (generated previously from virus stock cultures) diluted two-fold was used to generate a standard curve. The Ct values from the standard curve were used to interpolate the amount of SARS-CoV-2 RNA in each of the samples.

Statistical Analysis. All data were graphed as the mean \pm standard deviation (SD) using GraphPad Prism (v8.4). Data from at least two

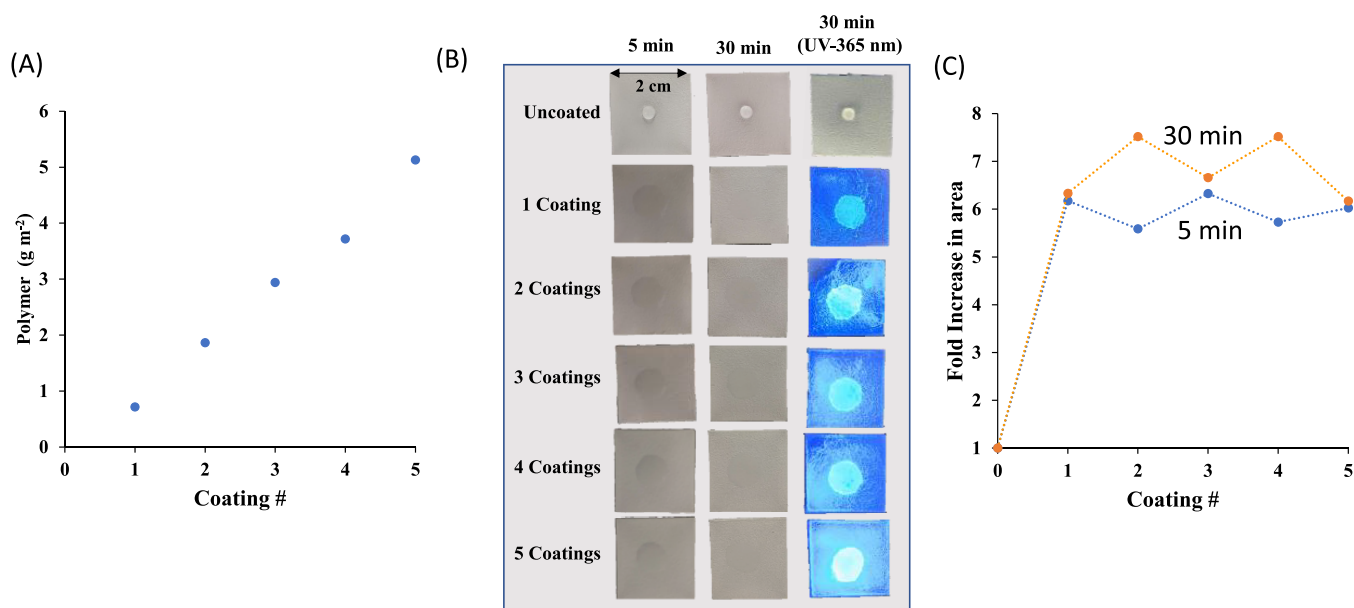


Figure 1. (A) Determination of the polymer per area of the surface with increasing amounts of coatings. (B) Spreading of a water droplet at pH = 6.5 on the coated surfaces. (C) Relative increase in droplet spreading with coating numbers.

independent experiments were pooled and graphed unless otherwise stated.

RESULTS AND DISCUSSION

The polymer nanostructures (i.e., with nanoworm morphology) were produced directly in water using the environmentally friendly emulsion polymerization method^{24,25} and further coupled with a variety of functional groups,²² including the hydrophobic octane (O), guanidine (G), a fluorescent probe (coumarin, C), and polygalactose (S), as shown in Scheme 1. We targeted binding to the highly glycosylated spike S protein²⁶ through (i) the strong multivalent binding with polygalactose and (ii) electrostatic interactions between the negatively charged viral particles and the positively charged guanidine and DMAEMA groups.²² The attached octane groups facilitate the rupture of the viral membrane, in which the viral mRNA can either be degraded by the guanidine groups or electrostatically captured by the polymer coating and degrade over time. Previously, we showed that these types of polymer nanoworms coated on surfaces, including a surgical mask, readily inactivated the influenza A virus, ancestral SARS-CoV-2 isolate (genetically matching the Wuhan/2019 strain), and the alpha variant.²² In this work, the polymer coating was tested against the highly transmissible and virulent delta and omicron variants to demonstrate its broad antiviral activity. We further wanted to determine whether a decrease in the amount of coating on the surface could still maintain virucidal activity, mimicking the loss of polymer coating on high-touch surfaces.

To demonstrate the scalability of the synthesis of the polymer nanoworms, the two macro-chain transfer RAFT poly(*N*-isopropylacrylamide) (PNIPAM) agents were produced from a single non-functional RAFT agent (Scheme 1). The emulsion polymerization using these two macro-chain transfer agents in the presence of styrene and initiated by AIBN at 70 °C in a 500 mL reactor produced spherical particles consisting of two block copolymers of MacroCTAs A and B with polystyrene at approximately 8 wt % of polymer in water (Scheme 1). After the addition of a small amount of plasticizer for polystyrene, the spherical nanoparticles trans-

formed into nanoworms upon cooling to room temperature. This process is denoted as the temperature-directed morphology transformation (TDMT) method,²⁴ which has been used successfully in our laboratory to produce a wide range of polymer nanoparticles ranging from worms,²⁵ vesicles,²⁴ toroids,²⁷ and tadpoles^{28,29} to stacked toroidal nanorattles.²⁷

The polymer nanoworms were then coupled to the functional groups (O, G, S, and C), dialyzed, freeze-dried, and then rehydrated with water to make a 1.5 wt % polymer/water dispersion. This polymer (NW_{S,O,C,G}) dispersion was then coated onto surfaces ranging from one to five sprays. The amount of polymer per area was determined by measuring the dry weight of polymer on the surface of a glass slide using a microbalance. With an increase in the number of sprays, the amount of polymer increased almost linearly from 1 to 5 g m⁻² (Figure 1A). Here, we carried out the emulsion polymerization at a 500 mL scale to produce approximately 40 g of polymer, and accordingly, the surface coverage can range from 8 to 40 m² with a decrease in the number of coatings from 5 to 1, respectively. Placing a water droplet at pH 6.5 on the coated surface (~2 × 2 cm) showed rapid spreading, visualized using the fluorescence at a wavelength of 365 nm (Figure 1B). The spreading increased approximately 6-fold compared to the uncoated surface, in which relatively no change in spreading was observed with increasing number of sprays after both 5 and 30 min (Figure 1C).

We next examined whether reducing the amount of nanoworm (NW_{S,O,C,G}) on the treated surface could maintain effective virucidal activity against the SARS-CoV-2 (alpha) VOC using the clinical human/Victoria/17991/2020 isolate.²² Sterile hard plastic surfaces were coated with one to five sprays of the nanoworms; then, virus inoculum (50 μL) prepared in Sorrenson's buffer pH = 6.5 was added dropwise onto the nanoworm-coated surface and incubated at room temperature for 30 min. Each surface was then washed with 10-fold media, and the eluate was collected and sampled immediately for viral genome extraction and for the presence of the SARS-CoV-2 infectious titer via performing a 50% tissue culture infectious dose (TCID₅₀) assay. We found in agreement with our

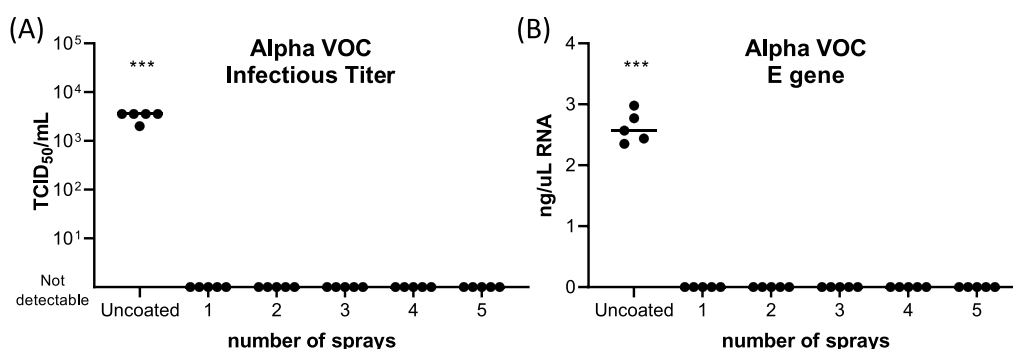


Figure 2. Virucidal activity of nanoworm-coated surfaces against SARS-CoV-2. Nanoworm-coated plastic hard surfaces or uncoated surfaces were exposed to SARS-CoV-2 human isolate Victoria/17991/2020 (Alpha VOC) for 30 min, then washed, and eluate-assayed for (A) the infectious SARS-CoV-2 titer by TCID₅₀ or (B) the presence of the intact SARS-CoV-2 E gene via quantitative RT-PCR. ****p* < 0.001 compared to all coatings, one-way ANOVA Dunnett's multiple comparison test.

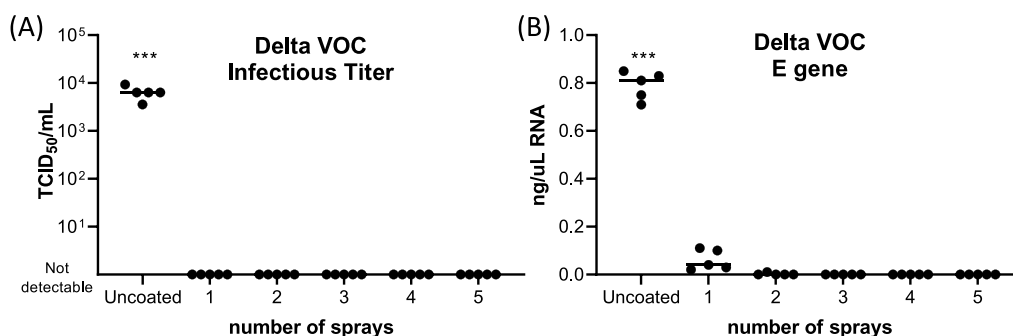


Figure 3. Virucidal activity of nanoworm-coated surfaces against SARS-CoV-2 delta VOC. Nanoworm-coated plastic hard surfaces or uncoated surfaces were exposed to SARS-CoV-2 human/Victoria/18440/2021 isolate with the identical genome to the delta (B.1.617.2) VOC for 30 min, then washed, and eluate-assayed for (A) the infectious SARS-CoV-2 titer by TCID₅₀ and for (B) the presence of the intact SARS-CoV-2 E gene via quantitative RT-PCR. ****p* < 0.001 compared to all coatings, one-way ANOVA Dunnett's multiple comparison test.

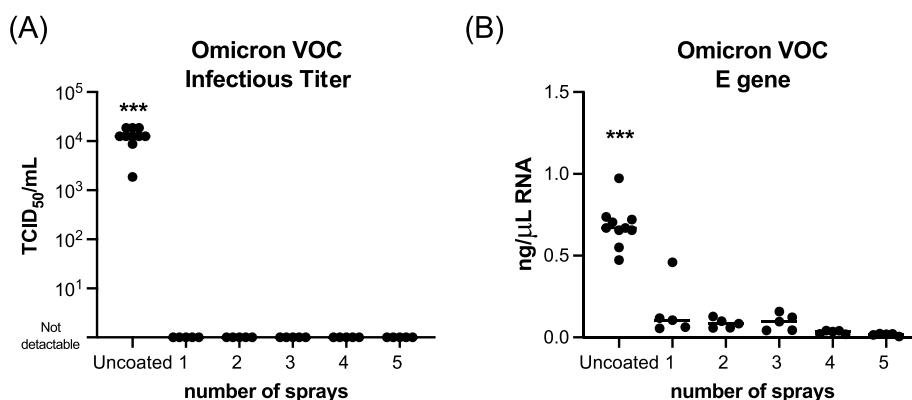


Figure 4. Virucidal activity of nanoworm-coated surfaces against SARS-CoV-2 omicron VOC. Nanoworm-coated plastic hard surfaces or uncoated surfaces were exposed to SARS-CoV-2 human/NSW/1933/2021 isolate with the identical genome to the omicron (B.1.1.529; BA.1 lineage) VOC for 30 min, then washed, and eluate-assayed for (A) the infectious SARS-CoV-2 titer by TCID₅₀ and for (B) the presence of the intact SARS-CoV-2 E gene via quantitative RT-PCR. ****p* < 0.001 compared to all coatings, one-way ANOVA Dunnett's multiple comparison test.

previous data²² that no detectable amount of infectious virus was observed, even after subsequent re-passaging in Vero cells to rescue any residual infectious virus (Figure 2A). As little as one spray on the surface was required to eliminate the presence of infectious virus within 30 min of exposure, demonstrating the effectiveness of the anti-viral polymer coating. To support the complete virucidal action of the nanoworm polymer, we performed quantitative RT-PCR for the presence of an intact E gene and found a significant reduction of virus genome detected regardless of the number of nanoworm sprays on the treated surface (Figure 2B).

We next tested the NW_{S,O,C,G} coating against the human/Victoria/18440/2021 isolate with the identical genome to the publicly available data of the original delta (B.1.617.2) virus isolate (www.gisaid.org, accession number: EPI_ISL_1913206). Upon examination of the predicted spike protein glycan array of the delta VOC and comparison to the ancestral virus,³⁰ the mutations in the spike protein were not expected to significantly change the glycosylation levels, and thus, we hypothesized that the delta VOC should have a similar ability to interact with our polymer nanoworm coating. To test this, and whether our polymer coating maintains

virucidal activity against the delta VOC, we repeated our assays using the delta VOC exposed to surfaces treated with one to five sprays of the nanoworm. Similar to the results obtained for the alpha VOC, the amount of infectious delta virus remaining in the eluate was below the detection limit, even after a second passage in the Vero cells (Figure 3A). Once again, as little as one spray was required to render the virus non-infectious, confirming the efficacy of this compound against SARS-CoV-2 variants. Complete inactivation of the delta VOC was further supported with the significant reduction of the intact viral E gene present in the sampled eluates (Figure 3B).

In comparison to the ancestral Wuhan SARS-CoV-2 isolate, the omicron SARS-CoV-2 VOC has a total of 60 mutations, with 37 (6 deletions, 1 insertion, and 30 substitutions) located in the spike protein.^{31,32} The omicron VOC has been reported to share 10 and 5 common mutations with alpha and beta variants, respectively, while seven mutations each were shared with the gamma and delta variants. Compared to the ancestral virus and delta VOC, the omicron spike protein is less efficiently cleaved and is less fusogenic,³³ indicating changed binding affinity and potential for enzymatic cleavage. Many of the spike mutations are within the important N-terminal domain, receptor binding domain, and receptor binding motif, raising concerns about enhanced transmission and immune evasion. Given the large number of mutations in omicron spike, we next evaluated whether our polymer could maintain its virucidal activity against this VOC. We repeated our assays using the omicron VOC (human/NSW/1933/2021; www.gisaid.org, accession number: EPI_ISL_3007291) exposed to surfaces treated with one to five sprays of the nanoworm. Importantly, as little as one spray of coating on the surface was sufficient to render the virus non-infectious as the eluate was found to be below the detection limit even after a second passage in the Vero cells and there was a significant reduction in the amount of detectable intact viral E gene (Figure 4A,B). This data further supports that the polygalactose targets binding to the glycosylated regions of the viral particles independent of the mutations presented on the spike.

The polymer nanoworms were then tested for both skin sensitivity on mice and oral ingestion toxicity in rats using ethically approved animal models to evaluate the potential safe use on masks and high-touch surfaces. These studies were carried out by an independent agent in compliance with the OECD Principle of Good Laboratory Practice. The skin sensitivity potential of NW_{S,O,C,G} was determined by administering 25 μ L of polymer as a topical application onto the dorsum of each ear of female CBA/CaH mice over a 6 day period (see Appendix S1 in the Supporting Information). On day 6, 20 μ Ci of ³H-thymidine was injected intravenously, and the auricular lymph nodes were dissected 5 h later. The stimulation index (SI) for the positive control (α -hexylcinnamaldehyde) was found to be 12.7, while the SIs for the polymer nanoworms at 2.5, 5, and 10 w/v % were 1.08, 1.24, and 1.42, respectively. An SI value greater than 3 represents a potential sensitizing agent. The non-clinical acute toxicity of NW_{S,O,C,G} was determined through a single bolus dose, ranging from 10 to 1000 mg/kg, in female Sprague Dawley rats (see Appendix S2 in the Supporting Information). Morbidity and mortality were observed daily during the acclimation period and twice daily after ingestion of the polymer over a 15 day period. There was no finding of either morbidity or mortality, with no changes in body weight or macroscopic pathology findings, supporting that the oral ingestion of the polymer was

well tolerated by the rats even with high doses of 1000 mg/kg. This combined data supports that the polymer nanoworms were non-toxic when ingested and did not cause irritation to the skin, supporting the potential use of the polymer in applications such as face coverings.

CONCLUSIONS

In summary, we have now shown that this functional water-borne and polymer system forms a transparent coating when applied directly to surfaces as a water solution to act as an effective virucidal agent that completely renders SARS-CoV-2 variants of concern non-infectious. The synthesis of polymer nanoparticles in water at 500 mL demonstrates the potential of the synthesis to be scaled to industrial amounts. The design of the polygalactose attached to the polymer nanostructure and potential specific bonding interactions with highly glycosylated SARS-CoV-2 provide a binding motif independent of the virus variant and mutations found in the virus spike attachment glycoprotein. The polygalactose binding in combination with the octane moieties and the responsive nature of the nanostructures that mechanically attach to and disrupt the viral particles renders them non-infectious. It was further shown that the SARS-CoV-2 viral RNA genome may either degrade as a result of the guanidine groups or be electrostatically captured by the cationic groups attached to the polymer that then allows for natural degradation. The fact that the viral RNA genome cannot be detected after interaction of the viruses with the polymer-coated surfaces demonstrates the complete virucidal activity of the polymer. We envisage that this polymer coating will provide inactivation of newly emerging SARS-CoV-2 VOCs with the ability to be re-designed to target other viruses. Finally, the polymer was found to be non-toxic by oral ingestion in rats and had little or no skin sensitization when applied on the skin of mice, indicating the potential use as a coating in personal protective equipment or high-touch point surfaces that comes into contact with the skin.

ASSOCIATED CONTENT

Supporting Information

The Supporting Information is available free of charge at <https://pubs.acs.org/doi/10.1021/acs.biomac.2c00801>.

The chemicals used, the synthesis of compounds and polymers, SECs, NMRs, FTIR, and TEMs (PDF)

ZIP file featuring the appendices of this work (ZIP)

AUTHOR INFORMATION

Corresponding Author

Michael J. Monteiro – Australian Institute for Bioengineering and Nanotechnology, The University of Queensland, Brisbane, QLD 4072, Australia; orcid.org/0000-0001-5624-7115; Email: m.monteiro@uq.edu.au

Authors

Valentin A. Bobrin – Australian Institute for Bioengineering and Nanotechnology, The University of Queensland, Brisbane, QLD 4072, Australia

Sung-Po R. Chen – Australian Institute for Bioengineering and Nanotechnology, The University of Queensland, Brisbane, QLD 4072, Australia; orcid.org/0000-0003-4257-3889

Carlos Fitzgerald Grandes Reyes – Australian Institute for Bioengineering and Nanotechnology, The University of Queensland, Brisbane, QLD 4072, Australia

Tim Smith – Department of Microbiology and Immunology, The University of Melbourne at the Peter Doherty Institute for Infection and Immunity, Melbourne 3000, Australia

Damian F. J. Purcell – Department of Microbiology and Immunology, The University of Melbourne at the Peter Doherty Institute for Infection and Immunity, Melbourne 3000, Australia

Jason Armstrong – Boeing Research and Technology Australia, Brisbane, QLD 4072, Australia

Julie L. McAuley – Department of Microbiology and Immunology, The University of Melbourne at the Peter Doherty Institute for Infection and Immunity, Melbourne 3000, Australia

Complete contact information is available at:

<https://pubs.acs.org/10.1021/acs.biomac.2c00801>

Author Contributions

[§]V.A.B. and S.-P.R.C. are co-first and equal authorship.

Funding

This work was supported by Boeing Pty Ltd.

Notes

The authors declare no competing financial interest.

REFERENCES

- (1) Barda, N.; Dagan, N.; Cohen, C.; Hernán, M. A.; Lipsitch, M.; Kohane, I. S.; Reis, B. Y.; Balicer, R. D. Effectiveness of a third dose of the BNT162b2 mRNA COVID-19 vaccine for preventing severe outcomes in Israel: an observational study. *Lancet* **2021**, *398*, 2093–2100.
- (2) Chemaitelly, H.; Tang, P.; Hasan, M. R.; AlMukdad, S.; Yassine, H. M.; Benslimane, F. M.; Al Khatib, H. A.; Coyle, P.; Ayoub, H. H.; Al Kanaani, Z.; Al Kuwari, E.; Jeremijenko, A.; Kaleeckal, A. H.; Latif, A. N.; Shaik, R. M.; Rahim, H. F. A.; Nasrallah, G. K.; Al Kuwari, M. G.; Al Romaihi, H. E.; Butt, A. A.; Al-Thani, M. H.; Al Khal, A.; Bertollini, R.; Abu-Raddad, L. J. Waning of BNT162b2 Vaccine Protection against SARS-CoV-2 Infection in Qatar. *New Engl. J. Med.* **2021**, *385*:e83.
- (3) Tang, P.; Hasan, M. R.; Chemaitelly, H.; Yassine, H. M.; Benslimane, F. M.; Al Khatib, H. A.; AlMukdad, S.; Coyle, P.; Ayoub, H. H.; Al Kanaani, Z.; Al Kuwari, E.; Jeremijenko, A.; Kaleeckal, A. H.; Latif, A. N.; Shaik, R. M.; Rahim, H. F. A.; Nasrallah, G. K.; Al Kuwari, M. G.; Al Romaihi, H. E.; Butt, A. A.; Al-Thani, M. H.; Al Khal, A.; Bertollini, R.; Abu-Raddad, L. J. BNT162b2 and mRNA-1273 COVID-19 vaccine effectiveness against the SARS-CoV-2 Delta variant in Qatar. *Nat. Med.* **2021**, *27*, 2136–2143.
- (4) Davies, N. G.; Abbott, S.; Barnard, R. C.; Jarvis, C. I.; Kucharski, A. J.; Munday, J. D.; Pearson, C. A. B.; Russell, T. W.; Tully, D. C.; Washburne, A. D.; Wenseleers, T.; Gimma, A.; Waites, W.; Wong, K. L. M.; van Zandvoort, K.; Silverman, J. D.; Diaz-Ordaz, K.; Keogh, R.; Eggo, R. M.; Funk, S.; Jit, M.; Atkins, K. E.; Edmunds, W. J. Estimated transmissibility and impact of SARS-CoV-2 lineage B.1.1.7 in England. *Science* **2021**, *372*, No. eabg3055.
- (5) Grange, Z.; Buelo, A.; Sullivan, C.; Moore, E.; Agrawal, U.; Boukhari, K.; McLaughlan, I.; Stockton, D.; McCowan, C.; Robertson, C.; Sheikh, A.; Murray, J. L. K. Characteristics and risk of COVID-19-related death in fully vaccinated people in Scotland. *Lancet* **2021**, *398*, 1799–1800.
- (6) Sheikh, A.; McMenemy, J.; Taylor, B.; Robertson, C.; Scotland, P. H.; Collaborators, E. I. SARS-CoV-2 Delta VOC in Scotland: demographics, risk of hospital admission, and vaccine effectiveness. *Lancet* **2021**, *397*, 2461–2462.
- (7) Baral, P.; Bhattarai, N.; Hossen, M. L.; Stebliankin, V.; Gerstman, B. S.; Narasimhan, G.; Chapagain, P. P. Mutation-induced changes in the receptor-binding interface of the SARS-CoV-2 Delta variant B.1.617.2 and implications for immune evasion. *Biochem. Biophys. Res. Commun.* **2021**, *574*, 14–19.
- (8) Planas, D.; Veyer, D.; Baidaliuk, A.; Staropoli, I.; Guivel-Benhassine, F.; Rajah, M. M.; Planchais, C.; Porrot, F.; Robillard, N.; Puech, J.; Prot, M.; Gallais, F.; Gantner, P.; Velay, A.; Le Guen, J.; Kassis-Chikhani, N.; Edriss, D.; Belec, L.; Seve, A.; Courtellemont, L.; Pere, H.; Hocqueloux, L.; Fafi-Kremer, S.; Prazuck, T.; Mouquet, H.; Bruel, T.; Simon-Loriere, E.; Rey, F. A.; Schwartz, O. Reduced sensitivity of SARS-CoV-2 variant Delta to antibody neutralization. *Nature* **2021**, *596*, 276–280.
- (9) Grabowski, F.; Preibisch, G.; Gizinski, S.; Kochanczyk, M.; Lipniacki, T. SARS-CoV-2 Variant of Concern 202012/01 Has about Twofold Replicative Advantage and Acquires Concerning Mutations. *Viruses* **2021**, *13*, 392.
- (10) Ziegler, C. G. K.; Allon, S. J.; Nyquist, S. K.; Mbano, I. M.; Miao, V. N.; Tzouanas, C. N.; Cao, Y. M.; Yousif, A. S.; Bals, J.; Hauser, B. M.; Feldman, J.; Muus, C.; Wadsworth, M. H.; Kazer, S. W.; Hughes, T. K.; Doran, B.; Gatter, G. J.; Vukovic, M.; Taliaferro, F.; Mead, B. E.; Guo, Z. R.; Wang, J. P.; Gras, D.; Plaisant, M.; Ansari, M.; Angelidis, I.; Adler, H.; Sucre, J. M. S.; Taylor, C. J.; Lin, B.; Waghay, A.; Mitsialis, V.; Dwyer, D. F.; Buchheit, K. M.; Boyce, J. A.; Barrett, N. A.; Laidlaw, T. M.; Carroll, S. L.; Colonna, L.; Tkachev, V.; Peterson, C. W.; Yu, A.; Zheng, H. B.; Gideon, H. P.; Winchell, C. G.; Lin, P. L.; Bingle, C. D.; Snapper, S. B.; Kropski, J. A.; Theis, F. J.; Schiller, H. B.; Zaragosi, L. E.; Barbry, P.; Leslie, A.; Kiem, H. P.; Flynn, J. L.; Fortune, S. M.; Berger, B.; Finberg, R. W.; Kean, L. S.; Garber, M.; Schmidt, A. G.; Lingwood, D.; Shalek, A. K.; Ordoval-Montanes, J.; Network, H. L. B. SARS-CoV-2 Receptor ACE2 Is an Interferon-Stimulated Gene in Human Airway Epithelial Cells and Is Detected in Specific Cell Subsets across Tissues. *Cell* **2020**, *181*, 1016–1035.e19.
- (11) Lukassen, S.; Chua, R. L.; Trefzer, T.; Kahn, N. C.; Schneider, M. A.; Muley, T.; Winter, H.; Meister, M.; Veith, C.; Boots, A. W.; Hennig, B. P.; Kreuter, M.; Conrad, C.; Eils, R. SARS-CoV-2 receptor ACE2 and TMPRSS2 are primarily expressed in bronchial transient secretory cells. *Embo. J.* **2020**, *39*, No. e105114.
- (12) Lee, B. U. Why Does the SARS-CoV-2 Delta VOC Spread So Rapidly? Universal Conditions for the Rapid Spread of Respiratory Viruses, Minimum Viral Loads for Viral Aerosol Generation, Effects of Vaccination on Viral Aerosol Generation, and Viral Aerosol Clouds. *Int. J. Environ. Res. Public Health* **2021**, *18*, 9804–9810.
- (13) Jackson, C. B.; Farzan, M.; Chen, B.; Choe, H. Mechanisms of SARS-CoV-2 entry into cells. *Nat. Rev. Mol. Cell Bio.* **2021**, *23*, 3–20.
- (14) Scudellari, M. How the coronavirus infects cells — and why Delta is so dangerous. *Nature* **2021**, *595*, 640–644.
- (15) Meyerowitz, E. A.; Richterman, A.; Gandhi, R. T.; Sax, P. E. Transmission of SARS-CoV-2: A Review of Viral, Host, and Environmental Factors. *Ann. Intern. Med.* **2021**, *174*, 69–79.
- (16) van Doremalen, N.; Bushmaker, T.; Morris, D. H.; Holbrook, M. G.; Gamble, A.; Williamson, B. N.; Tamin, A.; Harcourt, J. L.; Thornburg, N. J.; Gerber, S. I.; Lloyd-Smith, J. O.; de Wit, E.; Munster, V. J. Aerosol and Surface Stability of SARS-CoV-2 as Compared with SARS-CoV-1. *New Engl. J. Med.* **2020**, *382*, 1564–1567.
- (17) Riddell, S.; Goldie, S.; Hill, A.; Eagles, D.; Drew, T. W. The effect of temperature on persistence of SARS-CoV-2 on common surfaces. *Virol. J.* **2020**, *17*, 145–152.
- (18) Sia, S. F.; Yan, L. M.; Chin, A. W. H.; Fung, K.; Choy, K. T.; Wong, A. Y. L.; Kaewpreedee, P.; Perera, R. A. P. M.; Poon, L. L. M.; Nicholls, J. M.; Peiris, M.; Yen, H. L. Pathogenesis and transmission of SARS-CoV-2 in golden hamsters. *Nature* **2020**, *583*, 834–838.
- (19) Kratzel, A.; Steiner, S.; Todt, D.; V'Kovski, P.; Brueggemann, Y.; Steinmann, J.; Steinmann, E.; Thiel, V.; Pfaender, S. Temperature-dependent surface stability of SARS-CoV-2. *J. Infect.* **2020**, *81*, 452–482.

(20) Chin, A. W. H.; Chu, J. T. S.; Perera, M. R. A.; Hui, K. P. Y.; Yen, H. L.; Chan, M. C. W.; Peiris, M.; Poon, L. L. M. Stability of SARS-CoV-2 in different environmental conditions. *Lancet Microbe* **2020**, *1*, No. e10.

(21) Castaño, N.; Cordts, S. C.; Jalil, M. K.; Zhang, K. S.; Koppaka, S.; Bick, A. D.; Paul, R.; Tang, S. K. Y. Fomite Transmission, Physicochemical Origin of Virus-Surface Interactions, and Disinfection Strategies for Enveloped Viruses with Applications to SARS-CoV-2. *ACS Omega* **2021**, *6*, 6509–6527.

(22) Bobrin, V. A.; Chen, S. P.; Grandes Reyes, C. F.; Sun, B.; Ng, C. K.; Kim, Y.; Purcell, D.; Jia, Z. F.; Gu, W. Y.; Armstrong, J. W.; McAuley, J.; Monteiro, M. J. Water-Borne Nanocoating for Rapid Inactivation of SARS-CoV-2 and Other Viruses. *ACS Nano* **2021**, *15*, 14915–14927.

(23) Lee, J. Y. H.; Best, N.; McAuley, J.; Porter, J. L.; Seemann, T.; Schultz, M. B.; Sait, M.; Orlando, N.; Mercoulia, K.; Ballard, S. A.; Druce, J.; Tran, T.; Catton, M. G.; Pryor, M. J.; Cui, H. L.; Luttick, A.; McDonald, S.; Greenhalgh, A.; Kwong, J. C.; Sherry, N. L.; Graham, M.; Hoang, T.; Herisse, M.; Pidot, S. J.; Williamson, D. A.; Howden, B. P.; Monk, I. R.; Stinear, T. P. Validation of a single-step, single-tube reverse transcription loop-mediated isothermal amplification assay for rapid detection of SARS-CoV-2 RNA. *J. Med. Microbiol.* **2020**, *69*, 1169–1178.

(24) Kessel, S.; Urbani, C. N.; Monteiro, M. J. Mechanically Driven Reorganization of Thermoresponsive Diblock Copolymer Assemblies in Water. *Angew. Chem., Int. Ed.* **2011**, *50*, 8082–8085.

(25) Jia, Z.; Bobrin, V. A.; Truong, N. P.; Gillard, M.; Monteiro, M. J. Multifunctional Nanoworms and Nanorods through a One-Step Aqueous Dispersion Polymerization. *J. Am. Chem. Soc.* **2014**, *136*, 5824–5827.

(26) Li, F. Receptor Recognition Mechanisms of Coronaviruses: a Decade of Structural Studies. *J. Virol.* **2015**, *89*, 1954–1964.

(27) Jia, Z.; Bobrin, V. A.; Monteiro, M. J. Temperature-Directed Assembly of Stacked Toroidal Nanorattles. *ACS Macro Lett.* **2017**, *6*, 1223–1227.

(28) Bobrin, V. A.; Chen, S.-P. R.; Jia, Z.; Monteiro, M. J. Temperature-Directed Self-Assembly: from Tadpole to Multi-Arm Polymer Nanostructures Directly in Water. *ACS Macro Lett.* **2017**, *6*, 1047–1051.

(29) Bobrin, V. A.; Chen, S.-P. R.; Jia, Z.; Monteiro, M. J. Uniform Symmetric and Asymmetric Polymer Nanostructures via Directed Chain Organization. *Biomacromolecules* **2018**, *19*, 4703–4709.

(30) Casalino, L.; Gaieb, Z.; Goldsmith, J. A.; Hjorth, C. K.; Dommer, A. C.; Harbison, A. M.; Fogarty, C. A.; Barros, E. P.; Taylor, B. C.; McLellan, J. S.; Fadda, E.; Amaro, R. E. Beyond Shielding: The Roles of Glycans in the SARS-CoV-2 Spike Protein. *ACS Central Sci.* **2020**, *6*, 1722–1734.

(31) Rajpal, V. R.; Sharma, S.; Kumar, A.; Chand, S.; Joshi, L.; Chandra, A.; Babbar, S.; Goel, S.; Raina, S. N.; Shiran, B. 'Is Omicron mild?' Testing this narrative with the mutational landscape of its three lineages and response to existing vaccines and therapeutic antibodies. *J. Med. Virol.* **2022**, *94*, 3521–3539.

(32) Alkhatib, M.; Salpini, R.; Cariotti, L.; Ambrosio, F. A.; D'Anna, S.; Duca, L.; Costa, G.; Bellocchi, M. C.; Piermatteo, L.; Artese, A.; Santoro, M. M.; Alcaro, S.; Svicher, V.; Ceccherini-Silberstein, F. Update on SARS-CoV-2 Omicron Variant of Concern and Its Peculiar Mutational Profile. *Microbiol. Spectr.* **2022**, *10*, e02732–e02721.

(33) Suzuki, R.; Yamasoba, D.; Kimura, I.; Wang, L.; Kishimoto, M.; Ito, J.; Morioka, Y.; Nao, N.; Nasser, H.; Uriu, K.; Kosugi, Y.; Tsuda, M.; Orba, Y.; Sasaki, M.; Shimizu, R.; Kawabata, R.; Yoshimatsu, K.; Asakura, H.; Nagashima, M.; Sadamasu, K.; Yoshimura, K.; Genotype to Phenotype Japan (G2P-Japan) Consortium; Sawa, H.; Ikeda, T.; Irie, T.; Matsuno, K.; Tanaka, S.; Fukuhara, T.; Sato, K. Attenuated fusogenicity and pathogenicity of SARS-CoV-2 Omicron variant. *Nature* **2022**, *603*, 700–705.